Indian J Phys (May 2019) 93(5):603–610
https://doi.org/10.1007/s12648-018-1324-z

ORIGINAL PAPER

AC conductivity and conduction mechanism study of rubidium gadolinium diphosphate compound

S Mathlouthi*, A Oueslati and B Louati

Laboratory of Spectroscopic Characterisation and Optics of Materials, Faculty of Sciences, University of Sfax, B.P. 1171, 3000 Sfax, Tunisia

Received: 25 May 2018 / Accepted: 23 July 2018 / Published online: 13 October 2018

Abstract: The diphosphate $RbGdP_2O_7$ compound has been synthesized by the conventional solid-state reaction method and characterized by X-ray powder diffraction, Raman spectroscopy and impedance spectroscopy. The title compound crystallizes in the monoclinic system with $P2_1/c$ space group. The AC electrical conductivity was measured in a frequency range from 200 Hz to 1 MHz and temperature range 480–580 K. Impedance plot revealed the presence of two contributions at different temperatures associated with grain and grain boundary. The obtained results were analyzed by fitting the experimental data to an equivalent circuit model based on the ZView software. The temperature dependence of these contributions is found to obey the Arrhenius law with activation energies 0.42 eV and 0.32 eV, respectively. The alternating current (AC) conductivity of grain contribution follows the universal Jonscher's power law. The temperature dependency of frequency exponent 's' shows that the correlated barrier hopping model (CBH) is the most responsible mechanism for AC conduction in the investigated compound. The theoretical fitting between the proposed model and the experimental data showed good agreement.

Keywords: $RbGdP_2O_7$; X-ray diffraction; Ac conductivity; Conduction mechanism

PACS Nos.: 61.05.cp; 07.50.-e; 52.25.Mq; 78.20.Bh

1. Introduction

Over the past years, phosphate compounds have been the subject of numerous investigations for their potential applications in diverse areas such as solid-state laser materials, sensors, solid-state batteries, catalysts and ionic conductors [1–6]. Interestingly, diphosphate compounds with general formula $A^IM^{III}P_2O_7$ (where A^I is a monovalent cation and M^{III} rare earth element) have been a focal point due to their interesting conductivity coming from the mobile A^I ions located in the diphosphate group.

The essential structural feature of alkali rare earth diphosphates is a three-dimensional, cation–anion network having an interconnected interstitial space occupied by mobile A^I ions [7]. On the other hand, monovalent ions are responsible for the ionic conductivity properties that were observed in many compounds, with the attendant promise of applications such as solid electrolytes in rechargeable batteries [8–12].

Many investigations were carried out for these types of materials through these original properties and their good conductivity. Among the most interesting diphosphates, we have selected the $RbGdP_2O_7$ compound with tunnel structure where the Rb ions reside; this is a good character to supply a good conductivity.

A crystallographic study carried out by Parajón-Costa et al. revealed that $RbGdP_2O_7$ material is isostructural with KYP_2O_7 [13]. It crystallizes in the monoclinic system ($P2_1/c$ space group) with the following unit cell parameters: $a = 7.722$ Å, $b = 11.095$ Å, $c = 8.707$ Å, and $\beta = 105.281°$. The structural arrangement consists of corner-sharing GdO_6 octahedral and P_2O_7 diphosphate groups. The three-dimensional framework delimits tunnels running along [1 0 0] direction where the rubidium ions are located (Fig. 1).

The aim of this work is to report a detailed investigation on the electrical features of this compound as a function of frequency and temperature by using the impedance spectroscopy. Also, this study may give valuable information

*Corresponding author, E-mail: mathlouthi.samia92@gmail.com

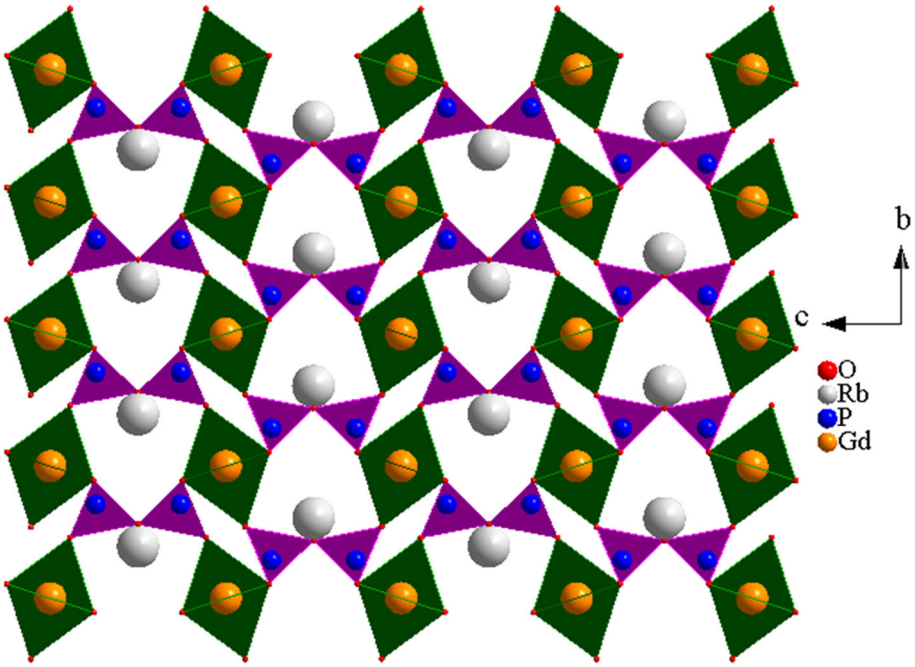

Fig. 1 Crystal structure of $RbGdP_2O_7$ compound

on the electrical conductivity and to determine the appropriate model responsible for the conduction mechanism.

2. Experimental details

The diphosphate $RbGdP_2O_7$ compound was obtained by the conventional solid-state reaction. The raw materials are Rb_2CO_3 (99.8%, Sigma-Aldrich), $NH_4H_2PO_4$ (99.999%, Sigma-Aldrich) and Gd_2O_3 (99.99%, Sigma-Aldrich). The starting reagents with their stoichiometric ratios were ground in an agate mortar and progressively heated from room temperature to 573 K in order to eliminate NH_3, H_2O and CO_2.

The resulting sample was reground, pelletized into cylindrical pellets using a hydraulic press at a pressure of 5 t/cm^2 and heated again at 800 K for 12 h in which the relative density obtained was 92%. The following reaction describes the synthesis of compound $RbGdP_2O_7$:

$$Rb_2CO_3 + Gd_2O_3 + 4(NH_4H_2PO_4) \rightarrow 2(RbGdP_2O_7) + 4NH_3 + CO_2 + 6H_2O$$

X-ray diffraction pattern was recorded at room temperature using a Philips PW1710 diffractometer operating with copper anticathode radiation CuK_α ($\lambda_{k\alpha}$ = 1.5418 Å) in a range of Bragg's angle $10° \leq 2\theta \leq 90°$. Unit cell parameters of the synthesized sample were refined with the Full Prof program by the least square method from the powder data.

The Raman spectrum was registered at room temperature in the wavenumber range (100–1400) cm^{-1} with a T-64000 Raman spectrometer (Horiba–Jobin–Yvon), using the 514.5-nm radiation of an Ar/Kr laser as excitation.

A pellet of 8 mm diameter and 1.2 mm thickness was used for electrical measurements. To obtain good contact, the pellet was covered on the opposite surfaces with a thin layer of gold and then mounted between two copper electrodes in a special holder. The performed measurements were taken in the frequency and temperature range of 200 Hz–1 MHz and 480–580 K, respectively, using an Agilent 4294 impedance analyzer.

3. Results and discussion

3.1. X-ray powder analysis

X-ray diffractogram (XRD) pattern of $RbGdP_2O_7$ recorded at room temperature is displayed in Fig. 2. Profile refinements using FoolProof suite program indicate that the resulting sample crystallizes in the monoclinic system with $P2_1/c$ space group. The estimated lattice parameters obtained from Rietveld analysis were found to be: a = 7.6917 Å, b = 11.0553 Å, c = 8.7778 Å and β = 105.13°. The reliability factors are: R_p = 18.1%, R_{wp} = 14.2% and χ^2 = 3.5. The refined lattice parameters of the compound are found to be very much consistent with those reported in the literature [13].

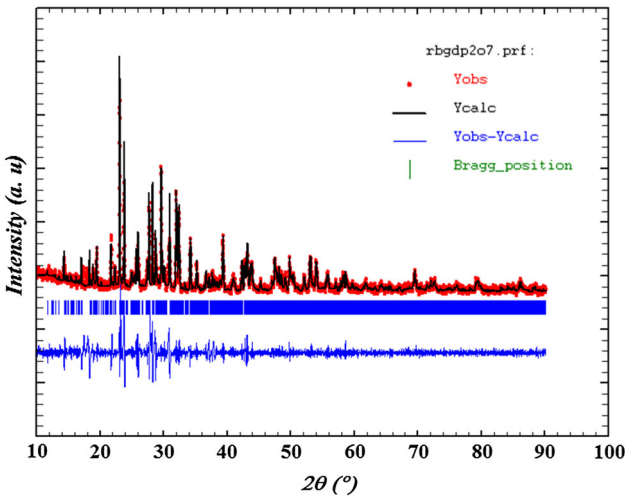

Fig. 2 The Rietveld refinement for $RbGdP_2O_7$ compound at room temperature. The dotted line indicates experimental data, and calculated data are represented by black continuous lines. The lowest curve in blue shows the difference between experimental and calculated patterns. The vertical bars in blue indicate the Bragg positions (colour figure online)

3.2. Raman spectroscopy

The Raman spectrum of $RbGdP_2O_7$ compound, obtained at room temperature, is shown in Fig. 3. A detailed assignment of the most important bands is dared by comparison with similar compounds [14–18]. The frequencies and proposed bands assignment are listed in Table 1. The frequencies of the P_2O_7 groups are attributed on the basis of the characteristic vibrations of the P–O–P bridge and PO_3 groups. Since the P-O bond in the PO_3 groups is stronger than that in the P–O–P bridge, we can note that the vibration frequencies of PO_3 are expected to be higher than those of P–O–P.

In fact, the bands observed at 1256, 1142 and 1100 cm^{-1} are attributed to the asymmetric ν_{as} (PO_3) stretching modes, whereas the symmetric stretching ν_s (PO_3) modes are found at the wavenumber 1072, 1041 and 987 cm^{-1}. The band related to the asymmetric stretching ν_{as} (POP) is detected at 719 cm^{-1}. The bands observed between 671 and 629 cm^{-1} are due to symmetric stretching vibration of ν_s (POP). As regards the deformation δ (PO_3) mode, it is identified in 574– 236 cm^{-1} region.

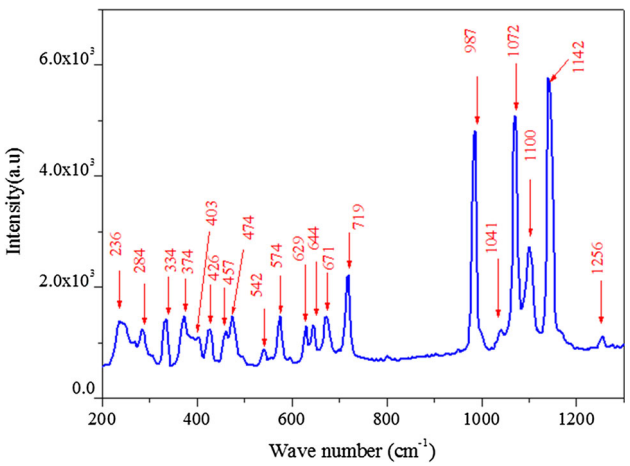

Fig. 3 Raman spectrum of $RbGdP_2O_7$ diphosphate

Table 1 Assignment of Raman bands for $RbGdP_2O_7$

Raman wavenumber (cm^{-1})	Assignments
1256; 1142; 1100	ν_{as} (PO_3)
1072; 1041; 987	ν_S (PO_3)
719	ν_{as} (POP)
671; 644; 629	ν_s (POP)
574, 542	δ (PO_3)
474; 457; 426; 403	
374, 334, 284, 236	

3.3. Impedance spectroscopy

Impedance spectroscopy is a useful technique to investigate, analyze and differentiate the role of different microstructures in the conduction process as each region has its unique electrical response within the chosen frequency and temperature domain. This technique allows the estimation grain and grain boundary's resistivity and capacitance [15, 19, 20].

Figure 4 represents the Nyquist plots ($-Z''(\omega)$ vs. $Z'(\omega)$) of $RbGdP_2O_7$ compound for several temperatures. All these plots are characterized by the presence of two semicircles revealing the existence of two contributions: the first, detected at high frequency, describes grain

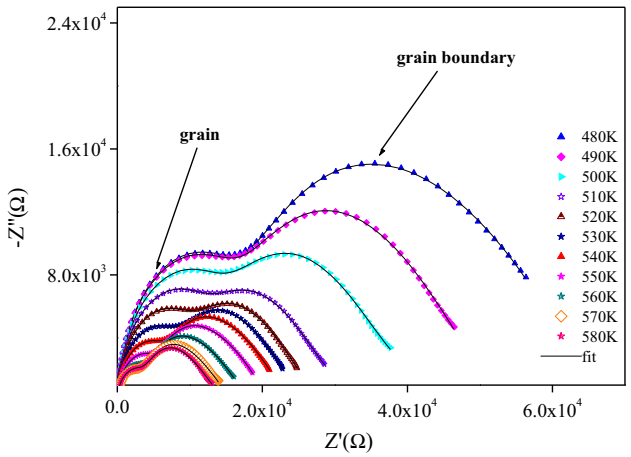

Fig. 4 The Nyquist plots of $RbGdP_2O_7$ compound different temperatures

contribution, while the second, at low frequency, is due to grain boundary one. The center of those semicircles is localized below the real axis (Z' axis), indicating a non-Debye-type relaxation [21]. ZView software was used to adjust the impedance data.

The best fits are obtained when we use an equivalent circuit (Fig. 5) that consists of a combination series of grains and grains boundary elements [22, 23]. The first consists of a parallel combination of resistance (R_1) and a constant phase element (CPE_1), while the second consists of a parallel combination of resistance (R_2), capacitance (C) and a constant phase element CPE_2. The impedance of CPE is: $Z_{CPE} = \frac{1}{Q(j\omega)^{\alpha}}$

The real (Z') and imaginary ($-Z''$) components of the impedance have been calculated, respectively, according to Eqs. (1) and (2):

$$Z' = \frac{R_1(1 + R_1Q_1\omega^{\alpha 1}\cos(\alpha_1\pi/2))}{(1 + R_1Q_1\omega^{\alpha 1}\cos(\alpha_1\pi/2))^2 + (R_1Q_1\omega^{\alpha 1}\sin(\alpha_1\pi/2))^2} + \frac{R_2^{-1} + Q_2\omega^{\alpha 2}\cos(\alpha_2\pi/2)}{(R_2^{-1} + Q_2\omega^{\alpha 2}\cos(\alpha_2\pi/2))^2 + (C\omega^{\alpha 2}\sin(\alpha_2\pi/2))^2} \quad (1)$$

$$-Z'' = \frac{R_1^2Q_1\omega^{\alpha 1}\sin(\alpha_1\pi/2)}{(1 + R_1Q_1\omega^{\alpha 1}\cos(\alpha_1\pi/2))^2 + (R_1Q_1\omega^{\alpha 1}\sin(\alpha_1\pi/2))^2} + \frac{C + Q_2\omega^{\alpha 2}\sin(\alpha_2\pi/2)}{(R_2^{-1} + Q_2\omega^{\alpha 2}\cos(\alpha_2\pi/2))^2 + (C\omega^{\alpha 2}\sin(\alpha_2\pi/2))^2} \quad (2)$$

where ω is the angular frequency, Q is the capacitance value of the CPE element, and α is the fractal exponent.

In order to confirm the choice of equivalent circuit, we present in Figs. 6 and 7 the variation of the experimental data of (Z') and (Z'') at several temperatures versus the simulated ones calculated using the parameters of the equivalent circuit. The superposition of these curves reveals a linear behavior with a slope substantially equal to the unity. This behavior indicates that the proposed equivalent circuit well describes the electric properties of the $RbGdP_2O_7$ compound.

The temperature dependence of the electrical conductivity of grain (σ_g) and grain boundary (σ_{gb}) is displayed in Fig. 8. It is clear from this figure that both σ_g and σ_{gb} conductivities increase with the rise in temperature, which

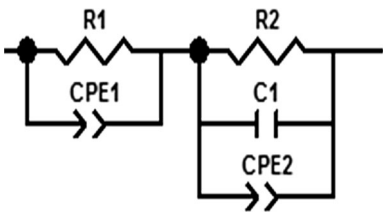

Fig. 5 The equivalent circuit model of the $RbGdP_2O_7$ compound

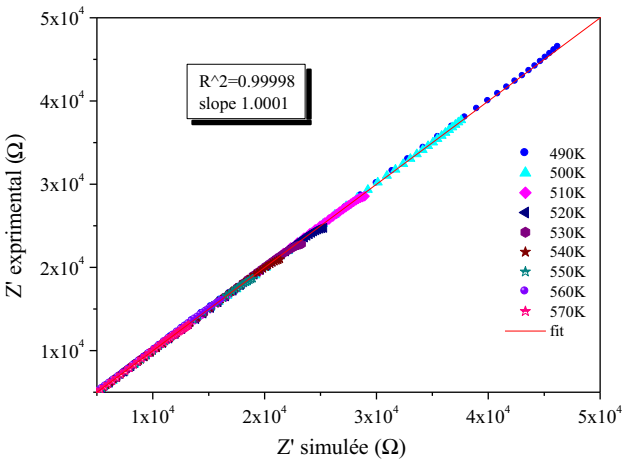

Fig. 6 Measured and simulated values of the real part of the complexes impedance

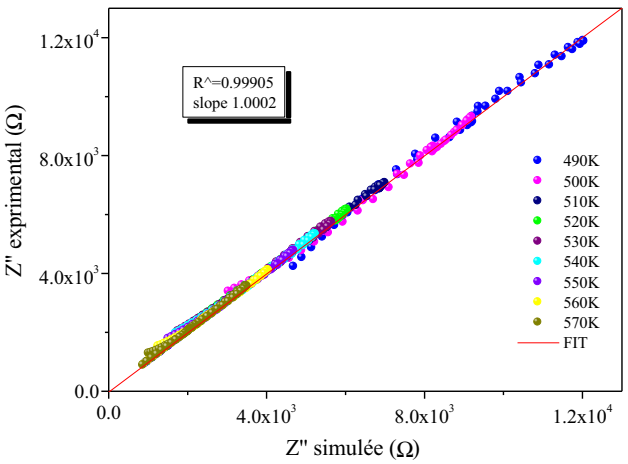

Fig. 7 Plot of experimental values versus simulated values of imaginary part Z''

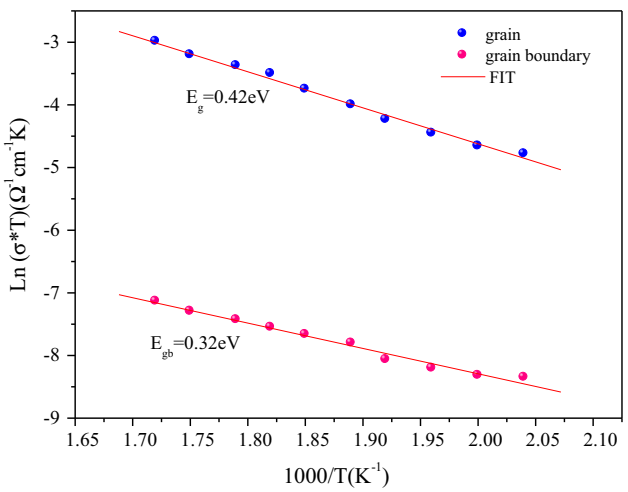

Fig. 8 Temperature dependence of Ln (σT) for $RbGdP_2O_7$

indicates a typical Arrhenius-type behavior in the sample [24]. The DC conductivity of grain and grain boundaries was calculated from Eqs. (3 and 4):

$$\sigma_g = \frac{e}{S * R_g} \tag{3}$$

$$\sigma_{gb} = \frac{e}{S * R_{gb}} \times \frac{C_g}{C_{gb}} \tag{4}$$

where e and S are, respectively, the thickness and the area of the pellet. The pure capacitance C can be obtained from the constant phase element CPE, using the following equation:

$$c_{gb} = R^{(1-\alpha)/\alpha} Q^{1/\alpha} \tag{5}$$

Following the Arrhenius law, the activation energy for bulk and grain boundary is found to be 0.42 eV and 0.32 eV, respectively. The obtained activation energy E_g is similar to those reported for semiconductor compounds [25, 26].

3.4. AC conductivity analysis

The frequency dependence of AC conductivity in RbGdP2O7 compound at different temperatures is plotted in Fig. 9. In some cases, the phenomenon of the AC conductivity dispersion is analyzed using the Jonscher's universal power law [27]:

$$\sigma_{ac} = \sigma_{dc} + A\omega^s \tag{6}$$

where σ_{dc} is the direct current conductivity, A is constant for a particular temperature, and s is an exponent less than or equal to unity which represents the degree of interaction between mobile ions and their surrounding lattices. An overview of the results (Fig. 9) unambiguously illustrates the existence of three distinct regions. In region *I*, at low frequency, the conductivity is almost constant. This is the evidence for the frequency-independent nature of the conductivity which represents the DC conductivity.

In the middle region of the figure, conductivity begins to increase nonlinearly due to the fact that capacitor admittance becomes numerically larger than resistor admittance with increasing frequency. However, for the third region, high-frequency domain, we notice that conductivity becomes proportional to frequency, involving loss approximately constant [28, 29].

Preliminary attempts to fit the conductivity results to Eq. (6) were unsuccessful. Thus, the frequency-dependent conductivity is analyzed by the following expression [30]:

$$\sigma_{ac}(\omega) = \frac{\sigma_s}{1+\tau^2\omega^2} + \frac{\sigma_\alpha \tau^2 \omega^2}{1+\tau^2\omega^2} + A\omega^s \tag{7}$$

where σ_s and σ_∞ are the conductivity values at low and high frequencies, respectively, τ is the characteristic relaxation time.

It is clear that experimental and fitted data are very close (Fig. 9). The frequency exponent s obtained by fitting the AC conductivity using Eq. (7) is plotted as a function of temperature in Fig. 10. It can be observed that the exponent s decreases from 0.46 at 490 K to 0.26 at 580 K. In general, the effect of temperature on the exponent (s) plays a key role in the estimation of conduction mechanism in disordered materials. According to the literature, there are different models [31–33] explaining the behavior of exponent s and its variation with frequency and temperature.

- Overlapping large-polaron tunneling (OLPT) model, wherein with the increase in temperature the exponent s first decreases, attains a minimum value and then increases.
- Non-overlapping small polaron tunneling (NSPT) model, wherein the exponent s increases with the increase in temperature.

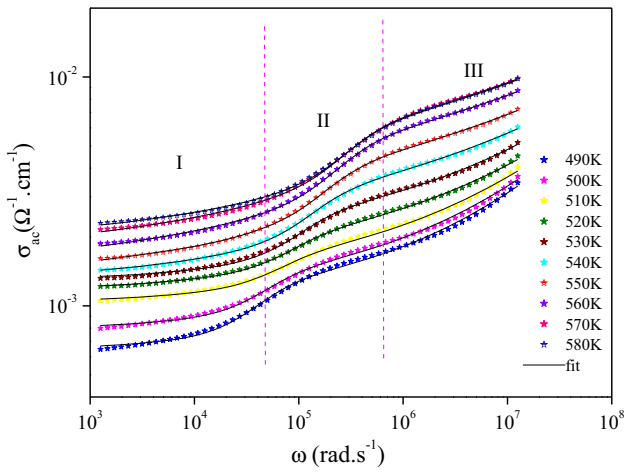

Fig. 9 Frequency dependence of AC conductivity at different temperatures

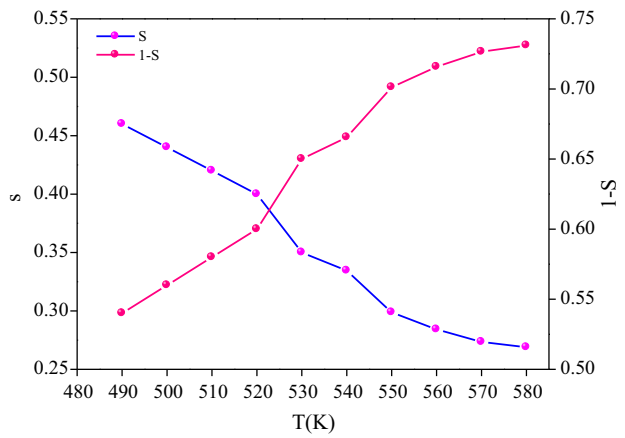

Fig. 10 Temperature dependence of the frequency exponent s

- Quantum mechanical tunneling (QMT) model, where the exponent s is independent of temperature and takes value equal to 0.8.
- Correlated barrier hopping (CBH) model, where the exponent s decreases with the increase in temperature.

In the present case, the temperature dependence of the exponent s for the studied sample is shown in Fig. 10, which clearly shows that s decreases with the increase in temperature. Consequently, the correlated barrier hopping (CBH) [34, 35] is in good agreement with our experimental results, suggesting, thus, that the electrical AC conduction mechanism of $RbGdP_2O_7$ compound can be explained by charge-carrier hops between sites over the potential barrier W_M separating them. In this model, carrier motion occurs by means of hopping over the Coulomb barrier separating two defect centers, and the AC conductivity is given by [36]:

$$\sigma_{ac}(\omega) = \frac{n}{24}\pi^3 N^2 \varepsilon' \varepsilon_0 \omega R_\omega^6 \tag{8}$$

where n is the number of polarons involved in the hopping process, N is the density of pair sites, and R_ω is the hopping distance for conduction ($\omega\ \tau = 1$) and is given by [37]:

$$R_\omega = \frac{e^2}{\pi\varepsilon\varepsilon_0\left[W_M - k_B T Ln\left(\frac{1}{\omega\tau_0}\right)\right]} \tag{9}$$

where W_M is the binding energy of the carrier in its localized sites and τ_0 is a characteristic relaxation time which is in the order of an atom vibrational period 10^{-13} s [38]. The power exponent s obeys the following relation [4]:

$$s = 1 - \frac{6k_B T}{\left[W_M - k_B T Ln\left(\frac{1}{\omega\tau_0}\right)\right]} \tag{10}$$

Equation (10) can be approximated to take the form:

$$s = 1 - \frac{6k_B T}{W_M} \tag{11}$$

The value of W_M is calculated as 0.21 eV from the slope of the straight line in Fig. 10. According to the CBH model, if the maximum barrier height W_M is the quarter of the activation energy (E_a), single polaron is the dominating conduction mechanism, while if $W_M = E_a/2$, the bipolaron hopping is the dominating [39]. From the above consideration, the maximum barrier height W_M is approximately the half of the activation energy which indicates that the bipolaron hopping is the dominating conduction mechanism.

The temperature dependence of AC conductivity for the titled compound is given in Fig. 11. Clearly, this figure shows that the theoretical calculations fitted by Eq. (8)

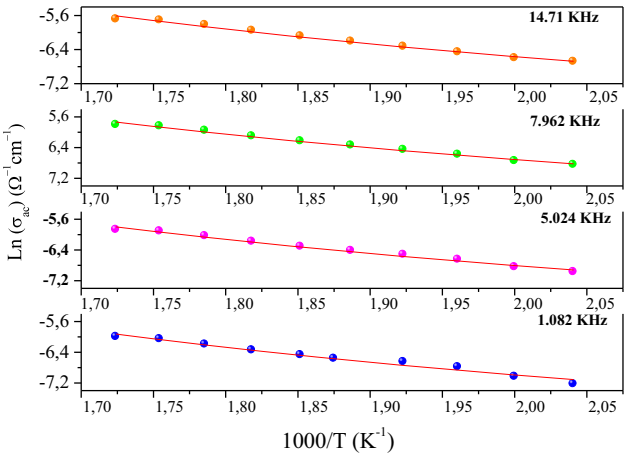

Fig. 11 Temperature dependences of σ_{ac} at different frequencies of $RbGdP_2O_7$

are good with the experimental results. It is evident from this figure that σ_{ac} increases linearly with the temperature, implying that the AC conductivity is a thermally activated process. The calculated fitting parameters are summarized in Table 2. From a qualitative analysis of these values, we can observe that an increase in the frequency causes a decrease in the states density localizes as shown in Fig. 12. Based on the definition given by Mott et al. [40], we can connect the reduction of the localized states density as a function of the frequency by the increase in the disorder, therefore diminishing the stabilities of states from which the non-localization of the latter occurs.

Figure 13 illustrates the variation of the tuning distance R_ω with temperature at selected frequencies. It is remarkable that R_ω increases with the increase in temperature, suggesting that the increase in temperature provides a contribution of thermal energy to polarons, which, afterward, will move and facilitate the hopping because of the interchain interaction that will occur. This is explained by the fact that the increase in the temperature induces a local disorder within the material. This disorder will, thus, favor the decrease in electrical conductivity.

The only conduction pathway is along tunnels in the a-direction, and the modest conductivity is determined by the dimensions of the tunnels section. So, further investigation on the relation of the electrical conductivity to structure for the $RbGdP_2O_7$ compound was done.

Table 2 Parameters used for CBH model fitting of $RbGdP_2O_7$

f (Hz)	N_T (cm^{-3})	W_M (eV)
1082	4.75 E^{21}	1.8
5024	4.01 E^{21}	1.72
7962	3.73 E^{21}	1.7
14,710	3.41 E^{21}	1.66

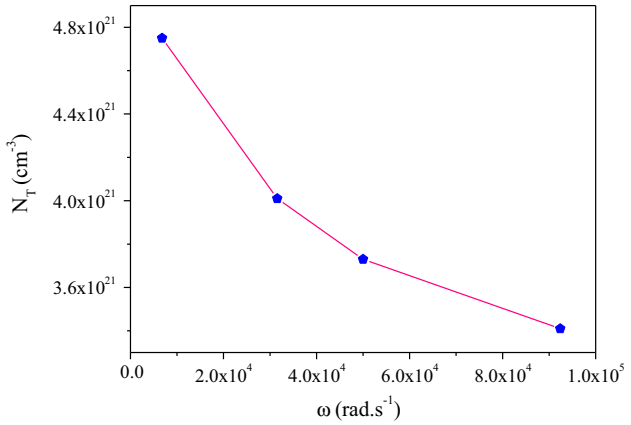

Fig. 12 Variation of parameter N_T (cm^{-3}) as a function of the frequency

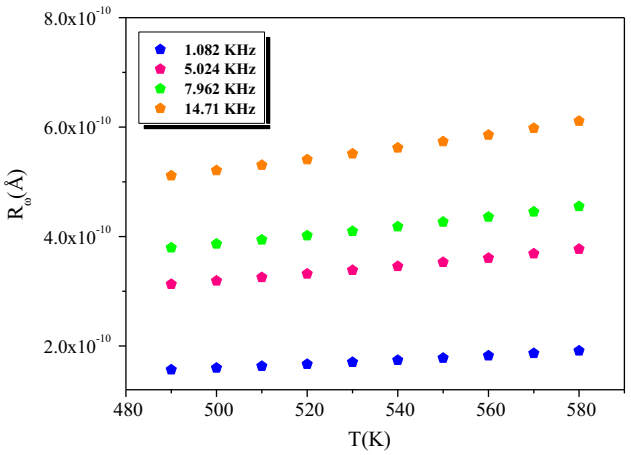

Fig. 13 Temperature dependence of the tunneling distance R_ω (Å) at different frequencies

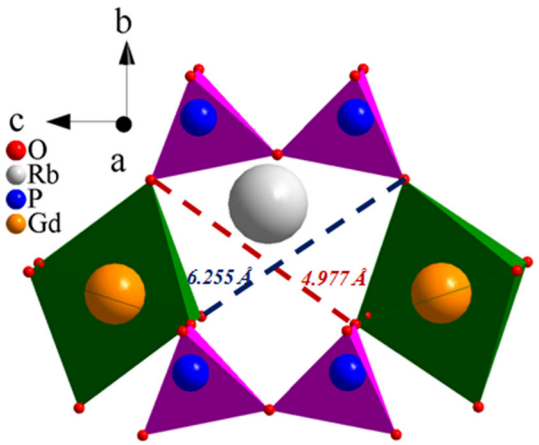

Fig. 14 View of the shape and size of the [1 0 0] tunnel sections

Consequently, as mentioned earlier, there is one kind of tunnels where Rb^+ cations are located. Based on the reported data [13] and using DIAMOND—Visual Crystal Structure software, we are able to present in Fig. 14. Otherwise, the dimensions of the tunnels vary between 4.977 and 6.255 Å, while, according to Shannon radii, the diameter of the rubidium ion is 3.32 Å [41]. We may conclude that this tunnel is of a sufficient dimension for ion transport. Thus, it can be deduced that the conduction process is assured by the movement of the Rb^+ cations along *a*-axis tunnels.

4. Conclusions

In summary, we have synthesized the $RbGdP_2O_7$ diphosphate by solid-state reaction. The X-ray diffraction analysis shows that the sample crystallizes in the monoclinic system with space group $P2_1/c$. The Raman spectrum was recorded and interpreted on the basis of the structural peculiarities of the $P_2O_7^{4-}$ moieties present in the crystal lattice. In addition, the impedance spectrum was described by two semicircles revealing the presence of two relaxations processes in the studied compound associated with the grain and grain boundary.

Consequently, an equivalent electrical circuit for the electrochemical cell with $RbGdP_2O_7$ was proposed. The AC conductivity for grain response is interpreted using the universal Jonscher's power law. The obtained activation energy for bulk is similar to those reported for semiconductor compounds.

Indeed, the temperature dependence of the exponent s shows that the correlated barrier hopping (CBH) model is the suitable model for explaining the AC conduction mechanism in the investigated compound.

Acknowledgements This work is financially supported by the Ministry of Higher Education and Scientific Research of Tunisia.

References

[1] B Louati, F Hlel and K Guidara *J. Alloys Compd.* **486** 299 (2009)
[2] M Megdiche, H Mahamoud, B Louati, F Hlel and K Guidara *Ionics* **16** 655 (2010)
[3] B Louati, M Gargouri, K Guidara and T Mhiri *J. Phys. Chem. Solids* **66** 762 (2004)
[4] Y Ben Taher, A Oueslati and M Gargouri *J. Alloys Compd.* **668** 206 (2016)
[5] R Ben Said, B Louati and K Guidara *Ionics* **20** 703 (2014)
[6] N Dridi, A Boukhari, J M Réau, E Arbib and E M Holt *Mater. Lett.* **47** 212 (2001)
[7] K Horchani-Naifer and M Férid *Solid State Ion.* **176** 1949 (2005)
[8] H Mahamoud, B Louati, F Hlel and K Guidara *J. Alloys Compd.* **509** 6083 (2011)
[9] V Biju and M A Khadar *J. Mater. Sci.* **36** 5779 (2001)
[10] B Louati and K Guidara *Ionics* **17** 633 (2011)
[11] S Nasri, M Megdiche and M Gargouri *Physica B* **451** 120 (2014)

[12] A Daidouh, M L Veiga, C Pico and M Martinez-Ripoll *Acta. Cryst.* C **53** 167 (1997)
[13] J L Yuan, J Wang, Z J Zhang, J T Zhao and G B Zhang *Opt. Mater.* **30** 132 (2008)
[14] B S Parajon-Costa, R C Mercader and E J Baran *J. Phys. Chem. Solid* **74** 354 (2013)
[15] H Mahamoud, B Louati, F Hlel and K Guidara *Bull. Mater. Sci.* **34** 1069 (2011)
[16] R Ben Said, B Louati and K Guidara *Ionics* **20** 1071 (2014)
[17] A B Rhaiem, S Chouaib and K Guidara *Ionics* **16** 455 (2010)
[18] E J Baran, R C Mercader, A Massaferro, E Kremer *Spectrochim. Acta. Part A* **60** 1001 (2004)
[19] M Idrees, M Nadeem and M M Hassan *J. Phys. D Appl. Phys.* **44** 155401 (2011)
[20] H Kchaou, A Ben Rhaiem, K Karoui and F Jomni *Appl. Phys. A* **122** 82 (2016)
[21] Y Ben Taher, A Oueslati, N K Maaloul, K Khirouni and M Gargouri *Appl. Phys. A* **120** 1537 (2015)
[22] M Ram *J. Alloys Compd.* **509** 5688 (2011)
[23] M Sassi, A Oueslati and M Gargouri *Appl. Phys. A* **119** 763 (2015)
[24] C R Mariappan, G Govindaraj, S Vinoth Rathan and G Vijaya Prakash *J. Mater. Sci. Eng. B* **121** 2 (2005)
[25] M I Youssif, F Sh Mohamed and M S Aziz *Mater. Chem. Phys.* **83** 250 (2004)
[26] S A El-Hakim, F A El-Wahab, A S Mohamed, and M F Kotkata. phys. stat. sol (a). **198**, 128 (2003)
[27] A K Jonscher, Dielectric Relaxation in Solids (1983)
[28] W Li and R W Schwartz *Appl. Phys. Lett.* **89** 242906 (2006)
[29] S Das, S Banerjee and T P Sinha *J. Nanosci. Nanotechnol. Res.* **1** 1 (2017)
[30] S Nasri, M Megdiche, K Guidara and M Gargouri *Ionics* **19** 1921 (2013)
[31] S Hassairi, B Louati and K Guidara *J. Alloys Compd.* **715** 397 (2017)
[32] S R Elliot *Adv. Phys.* **36** 135 (1987)
[33] A Ghosh *Phys. Rev. B* **41** 1479 (1990)
[34] R Punia, R S Kundu, M Dult, S Murugavel and N Kishore *J. Appl. Phys.* **112** 083701 (2012)
[35] S Nasri, A Oueslati, I Chaabane and M Gargouri *Ceram. Int.* **42** 14041 (2016)
[36] N Mehtaa, D Kumarb, S Kumarc and A Kumard *Chalcogenide Lett.* **2** 103 (2005)
[37] A Kahouli, A Sylvestre, F Jomni, B Yangui and J Legrand *J. Phys. Chem. A* **116** 1051 (2012)
[38] S R Elliott *Adv. Phys.* **36** 135 (1987)
[39] S Hajlaoui, I Chaabane and K Guidara *RSC Adv.* **6** 91649 (2016)
[40] N F Mott, E A Davis, 2nd edn. Clarendon Press, Oxford (1979)
[41] R D Shannon *Acta. Cryst. Sect. A* **32** 751 (1976)